Polymer 50 (2009) 6157–6165

Contents lists available at ScienceDirect

Polymer

journal homepage: www.elsevier.com/locate/polymer

Macromolecular effect on crystal pattern formation in ultra-thin films: Molecular segregation in a binary blend of PEO fractions

Liuxin Jin, Guoliang Zhang, Xuemei Zhai [1], Zhenpeng Ma, Ping Zheng, Wei Wang*

The Key Laboratory of Functional Polymer Materials of Ministry of Education and Institute of Polymer Chemistry, College of Chemistry, Nankai University, Tianjin 300071, China

ARTICLE INFO

Article history:
Received 20 July 2009
Received in revised form
13 October 2009
Accepted 19 October 2009
Available online 24 October 2009

Keywords:
Pattern formation
Polymer blends
Crystallization

ABSTRACT

In this work we report our investigation on the crystal patterns of a 50/50 blend of two polyethylene oxide (PEO) fractions with different molecular weights ($\overline{M}_w =$ 5040 and 35000 g/mol) in ultra-thin films. Using AFM with a hot stage the samples on the surface of silicon wafer were isothermally crystallized at $20.0 \leq T_c \leq 60.0\,^{\circ}C$. The crystal patterns are different from those of the two pure fractions. Co-crystallization, partial segregation and full segregation have been observed. Especially, within $47.0 \leq T_c \leq 54.0\,^{\circ}C$ dual thickness crystals formed. The thickness of the middle part of the crystal corresponds to the lamella thickness of 35k-PEO fraction with multiple folds, while the thickness of the edge part is nearly equal to an extended-chain lamella thickness of 5k-PEO fraction. We suppose that the appearance of the dual thickness crystals is due to molecular partial segregation. Utilizing in-situ AFM, the growth of the crystal with dual thicknesses as a function of time was monitored at $T_c = 54.0\,^{\circ}C$. Two growth processes were observed and a pattern formation mechanism was suggested on the basis of specified molecular motion and chain-fold crystallization of polymers.

1. Introduction

In polymer science molecular mass and its distribution are the most important parameters because they strongly influence physical structures as well as properties of synthetic polymer materials. In crystallization, for instance, molar mass has been found to have dramatic effect on the crystallization capability and crystal morphology characteristics [1–3]. Crystallization of most polymers is accompanied by the separation of molecules with different masses [4–11]. This process is referred to as molecular segregation or molecular fractionation, distinguished from small molecules. The experimental investigations on polyethylene (PE) [4–7] and poly(ethylene oxide) (PEO) [8–11] have shown that molecular segregation in the mixtures occurs before the temperature reaches the equilibrium melting point of the low molecular weight fraction. By separating rejected molecules from the bulk crystal after the completion of crystal growth and then determining the molar mass, Mehta and Wunderlich indicated that there exists a critical molar mass (M_{crit}) at a certain crystallization temperature (T_{crit}). The macromolecules, with molecular mass larger than M_{crit}, are able to crystallize at this crystallization temperature. Fig. 1 is a schematic diagram of the crystallization behavior of binary mixtures of two linear fractions [2]. In this diagram, H and L mean the high and low molecular mass fractions. The temperature T_1 is the upper crystallization temperature (T_c) for H fraction. At $T_2 \leq T_c \leq T_1$ sole crystallization of H fraction causes a full segregation. Thus, for L fraction, T_2 is T_{crit}, but T_2 is not the equilibrium melting point of L fraction. At temperatures below T_2, H and L fractions both crystallize but in separate crystal lamellae, which indicates a partial segregation occurs. Some limited co-crystallization without any molecular segregation occurs at very low crystallization temperatures. Co-crystallization is the term applied to the process that both polymers crystallize in the same crystal lamella. This diagram has been confirmed by many experimental observations in bulk samples of the binary mixtures of PEOs [8–11]. DSC and SAXS were employed to study whether the components crystallize separately or together. Optical microscopy and TEM provided the most direct information about segregation phenomena. It has been observed that in partial segregation range, the long chain fractions are enriched in the early-grown thick crystals of spherulites while the short chain fractions are rich in the later-grown thin crystals. Molecular nucleation, the process that each molecule has to go through a nucleation stage before it is

* Corresponding author.
E-mail addresses: jlx115@mail.nankai.edu.cn (L. Jin), guoliang2008@mail.nankai.edu.cn (G. Zhang), zhaixmei@mail.nankai.edu.cn (X. Zhai), mazhenpeng@mail.nankai.edu.cn (Z. Ma), zhengping@nankai.edu.cn (P. Zheng), weiwang@nankai.edu.cn (W. Wang).
[1] Present address: Microscopy/Thermal Analytical Science, Asia Pacific Research, Dow Chemical (China) Investment Co. Ltd., 5/F, No. 512 Yutang Road Building C, Songjiang Industrial Park, Shanghai 201613, China.

0032-3861/$ – see front matter © 2009 Elsevier Ltd. All rights reserved.
doi:10.1016/j.polymer.2009.10.041

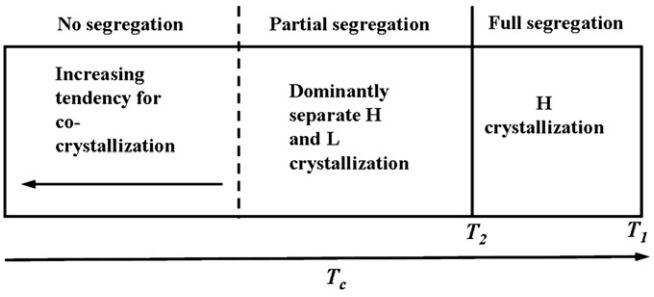

Fig. 1. Schematic diagram showing the crystallization behavior of binary mixtures of two fractions.

accepted into the crystal, has been suggested to explain the molecular segregation phenomenon. Recently, an evidence of molecular simulations to identify molecular segregation in the supercooled regions has been given by Hu and coworkers [12,13]. Fig. 1 has been further reconfirmed; besides, the model of intramolecular nucleation is employed to quantitatively interpret the kinetics-controlled molecular segregation.

In the conditions far from equilibrium, diverse crystallization patterns, such as dendrite, seaweed, and compact structure have been observed and the investigation on their formation nature has attracted great attention of scientists working in the fields of statistical physics and condensed matter physics [14–19]. Nowadays, it is well known that the formation of these patterns is due to the crystal growth instability caused by a diffusion field with different boundary conditions [14–23]. The further studies have demonstrated patterns change when boundary conditions altered gradually [24–28]. In recent years, seaweed, dendrite and faceted crystal patterns have also been found in the ultra-thin samples of some semicrystalline polymers [29–45]. Since molecular motion and crystallization behavior of polymers highly depend on molecular mass, these studies are supposed to elucidate the macromolecular effects on the formation and transition of crystal patterns.

In this study, we pay our attention to the crystal pattern formation of polymer blends in ultra-thin films. With regard to polymer blends, miscibility and phase segregation have been the subjects of intensive studies for a long time, with both applicative and comprehensive objectives and recently scientists give more attention to the morphology phase diagram of polymer blends [46–48]. Our purpose is to have a depth comprehension of molecular segregation in polymer ultra-thin films that was considered to be negligible because of the topological constraint [49]. In order to explore the effect, we studied crystal patterns of a binary blend of two PEO fractions with weight molar masses of 5040 and 35,000 g/mol (denoted as 5k-PEO and 35k-PEO hereafter) on the surface of silicon wafer using AFM with a hot stage. Our observations show seaweed, fourfold-symmetrical structure and faceted crystals in the studied temperature range. Interestingly, they are greatly different from those of pure 5k-PEO and 35k-PEO fractions at the same crystallization conditions. More significantly, we find that molecular partial segregation in the binary blend results in special crystal patterns with dual thicknesses. The selection of these patterns further reflects a growth competition of the macromolecules with different molecular weights because of their diverse abilities of molecular motion and nucleation-growth.

2. Experimental section

2.1. Materials and sample preparation

PEO fractions used were purchased from Fluka. Their characterization data are listed in Table 1. Both components contain a methyl group at one end and a hydroxyl group at the other end. The maximum length, L, of 5k-PEO molecules in the fully extended form is $L = l_m N = 31.6$ nm where the repeating unit length is $l_m = 0.2783$ nm [50–52], and the degree of polymerization is $N = 114$. This PEO may form chain-folded lamellae with integral folds so the lamellar thickness is $l(n) = L/(n+1)$, where n is the number of folds [52] and the folded chain lamella has a zero-entropy-production melting temperature $T_m(n)$. As to 35k-PEO, the degree of polymerization is $N = 795$, so normally it forms the non-integer chain-folded lamellae.

The as-received materials were used without further purification. The blend sample with a weight ratio of 50/50 was prepared from toluene solution of the two PEO fractions. The fractions were weighed respectively with the same mass and then dissolved into the toluene at a concentration of about 0.01 wt% under continuous stirring. The silicon wafers were cleaned at first by immersing in a solution of H_2SO_4 (98%):$H_2O_2 = 3{:}1$ at 120 °C for 30 min to remove any organic contamination and then cleaned in an ultrasonic water bath. The silicon surface became hydrophilic as the static contact angle measured with water is about 8°. The thin PEO films on the surface of silicon wafers were prepared simply by dropping polymer solution at room temperature after annealing for 6 h at 70 °C in order to obtain a uniform distribution solution before use. To keep a solvent-saturated atmosphere around the sample and to allow uniform evaporation, a glass dome was placed on the top of the sample after dropping the solution. The resulting films were further dried in vacuo for 12 h, and the thickness of prepared films is about 3–4 nm [43,44,53]. Normally, a monolayer of flat-on crystals with fractal-like patterns formed on the wafer surface. Finally, the samples were heated to 80.0 °C for 5 min on the hot stage of AFM to melt any crystals formed during drying and then recrystallized in the selected T_c.

2.2. Instruments and data analysis

A hot stage multimode atomic force microscope (AFM, Digital Instrumental Nanoscope IV) was used to visualize crystal patterns. All measurements were performed in tapping mode. Both height and phase images were recorded simultaneously. The scan rate was in the range 1.0–2.0 Hz. The temperature of the hot stage can be precisely controlled within ±0.1 °C. The temperature preset and the height measured were calibrated using the standard samples provided by Digital Instruments. Since the hot stage was used in a relatively moderate temperature region and the PEO film samples were very thin, the AFM tip effect on film temperature is trivial. Thus, no further calibration on the tip effect was carried out [54]. For each sample, at least three replicate samples were prepared and on each sample, a minimum of five different areas on the surface were investigated to ensure a good reproducibility of the AFM observations.

The digital images were used to determine the fractal dimension, D_p, of the crystal patterns according to the dilation method [55,56] And the definition of the fractal dimension of the curve is $N(r) \propto r^{-D_p}$, where N is the number of segments that are needed to approximate the curve and r the length of segments. In Euclidean

Table 1
Molecular weight, $\overline{M}_w$, polydispersity, $\overline{M}_w/\overline{M}_n$, and equilibrium melting points, $T_m^0(MW)$, of two PEO fractions.

Sample	$\overline{M}_w$ (g/mol)	$\overline{M}_w/\overline{M}_n$	$T_m^0(MW)$ (°C)[a]
35k-PEO	3.50×10^4	1.23	67.8
5k-PEO	5.04×10^3	1.01	62.2

[a] Calculated using the Flory-Vrij relation in Refs. [64] and [65].

geometry $D_p = 1$ [55,56,57]. All of the images were shown without any image processing except flattening.

3. Results and discussion

3.1. Patterns and transitions

In our previous studies [37,45], we have investigated the crystal patterns of the 5k-PEO and 35k-PEO fractions, respectively. Our previous studies demonstrate that the pattern formation of PEO crystals is highly dependent on the crystallization temperature. According to previous works [4–11], we know that molecular segregation occurs within a specified temperature range as schematically shown in Fig. 1. Therefore, our AFM observations were performed in a temperature range from 20.0 to 60.0 °C. The AFM images in Fig. 2 show different crystal patterns formed by the blend in this temperature range. At $20.0 \le T_c \le 28.0$ °C the typical seaweed pattern is found of which the angles between main and side branches are not a constant. At $28.0 < T_c < 47.0$ °C the crystal pattern is a typical dendrite of which feature is 90° angles between main and side branches. And we consider that anisotropic growth causes the formation of the dendrite pattern; while the random sticking process results in the seaweed pattern [15]. At $47.0 \le T_c \le 54.0$ °C the crystal patterns have a fourfold-symmetric (FS) structure without any large side branches. Their feature is greatly altered with a one-degree temperature increment. The most fascinating feature of these patterns is that the periphery of the patterns seems to be fabricated by many small squares. The size of these square crystals becomes larger with increasing distance to the center. At $T_c = 56.0$ °C the pattern no longer has the FS structure and seems to be formed by a couple of larger square crystals. At $T_c = 58.0$ °C faceted crystals with approximate square or rectangle shape are found.

In Fig. 3, we select the crystal patterns of three samples obtained at $T_c = 30.0$, 48.0 and 52.0 °C to represent the pattern differences among neat components and the blend. For the 5k-PEO fraction we see dendrite at $T_c = 30.0$ °C, seaweed at $T_c = 48.0$ °C and an ill-shaped structure at $T_c = 52.0$ °C. For the 35k-PEO fraction we observe a labyrinth pattern at $T_c = 30.0$ °C, dendrite at $T_c = 48.0$ and 52.0 °C. While, with regard to the blend, seaweed crystals exist at low temperature, and square-crystal-inlaying FS structure can be found at the other two temperatures. It is obvious that in the PEO blend crystallization, the two components cannot crystallize respectively without interaction. This clearly indicates molecular weight and polydispersity of polymers can significantly affect the polymer crystallization in ultra-thin films.

3.2. Quantitative description of patterns

To have a quantitative description of patterns and their temperature dependence, their fractal dimension, D_p and thickness are determined. Fig. 4 shows the T_c-dependence of D_p for the

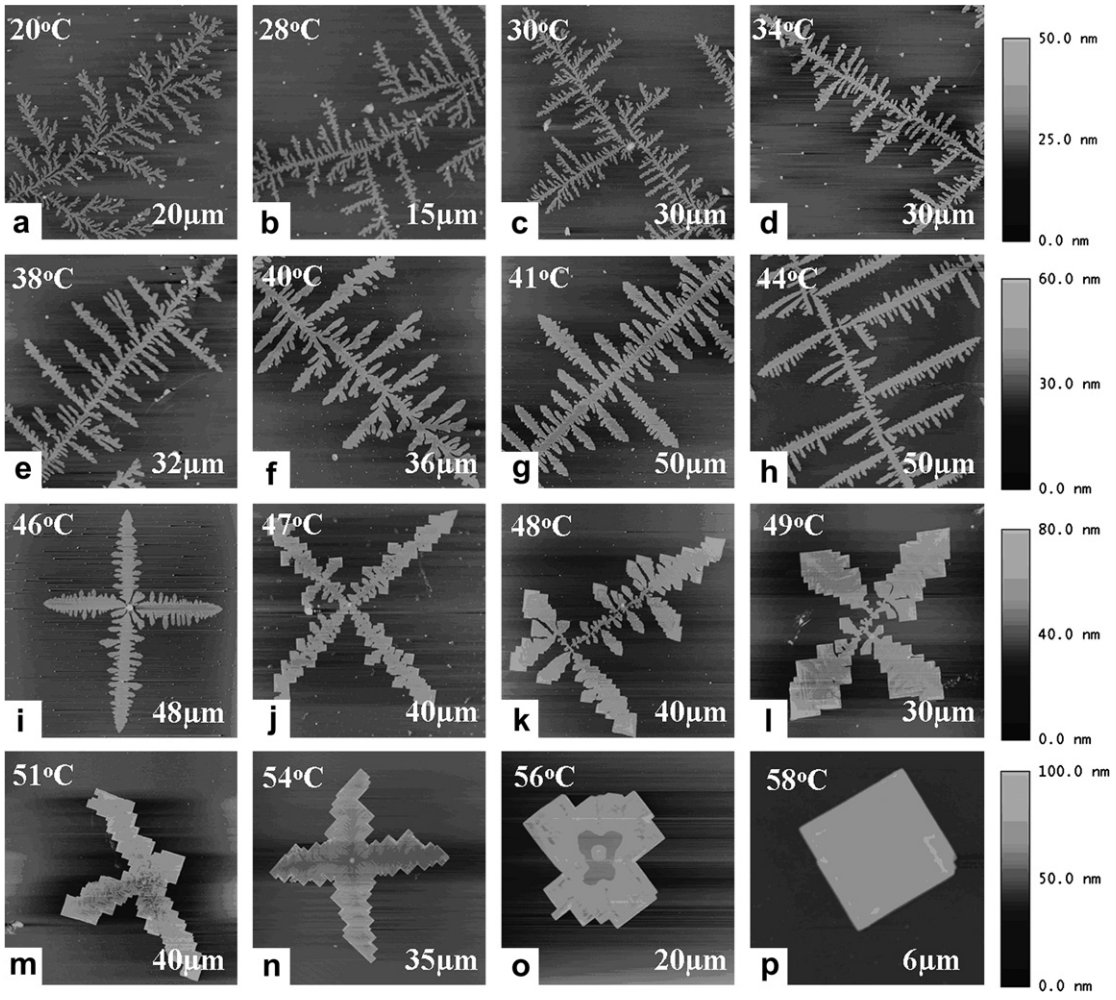

Fig. 2. AFM height images showing the different crystal patterns of the blend obtained at different crystallization temperatures.

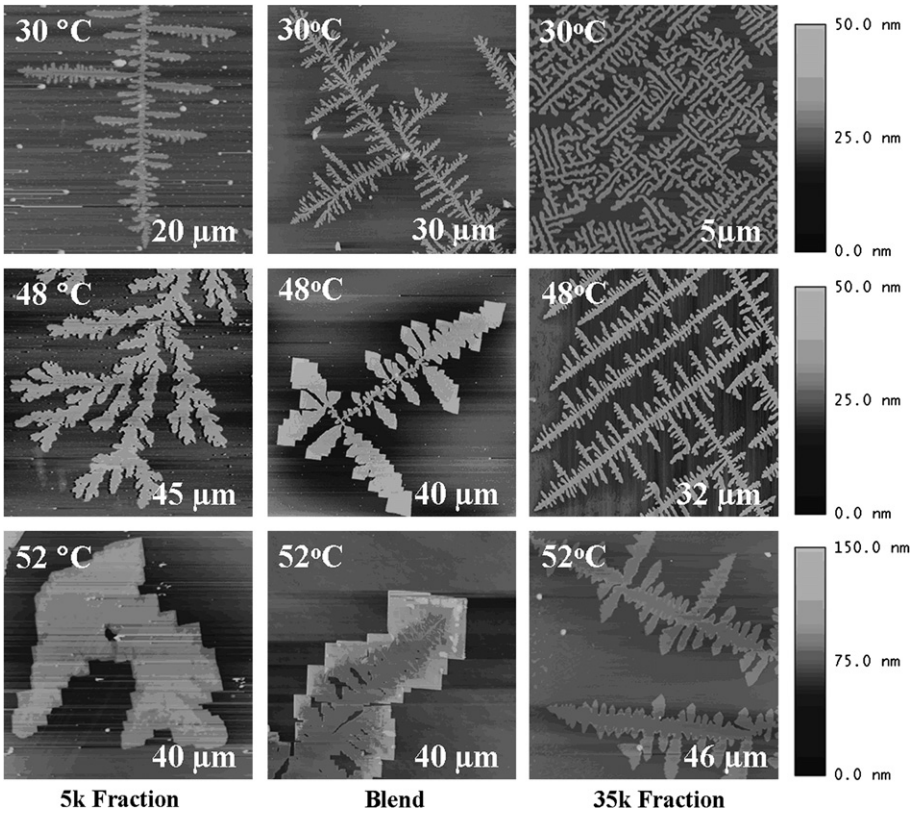

Fig. 3. Crystal patterns of the pure fractions and their blend obtained at the same crystallization temperature.

blend sample as well as the two neat fractions for comparison. The T_c-dependences of D_p can be fitted by a Sigmoidal function. The inflexion temperatures are 51.9 °C for the blend, 49.9 °C for the 5k-PEO fraction and 54.2 °C for the 35k-PEO fraction, respectively. The wide transition range and the deviation from the fitting curve for the blend can be explained by the wide molecular mass distribution. However, the T_c-dependences of D_p for three samples all can be divided into three regions, which reveals the common characteristics of crystal patterns for three samples. In the lower T_c region, three samples have the similar fractal dimension $D_p = 1.68 \pm 0.02$ on average. This is the typical fractal dimension of patterns created by diffusion limited aggregation (DLA) model [20,21,57]. It means that the instability of crystal growth in a diffusion field is the major mechanism governing the pattern formation. With further increasing T_c, the D_p value reduces from 1.54 to 1.30, indicating a gradual losing of the fractal feature and that is corresponding to a crystal pattern transition from the ramified pattern to a FS structure. At higher crystallization temperatures, the D_p value reduces approximately to 1.0, suggesting the formation of the faceted crystals. And we consider that it is controlled by surface kinetic process [25]. In this case, molecules have already moved to the growth front and will select the best position with the largest number of occupied nearest neighbor to join the crystal, which can lower the surface free energy. Therefore, it is prone to form regular shape patterns for polymer in ultra-thin films when T_c is high. At intermediate temperatures, diffusion mechanism and surface kinetic process both have contribution to the gradual loss of fractality of patterns. Thus, from macroscopic aspect, the mechanisms that govern the pattern formation and transition are similar, no matter neat fractions or blend.

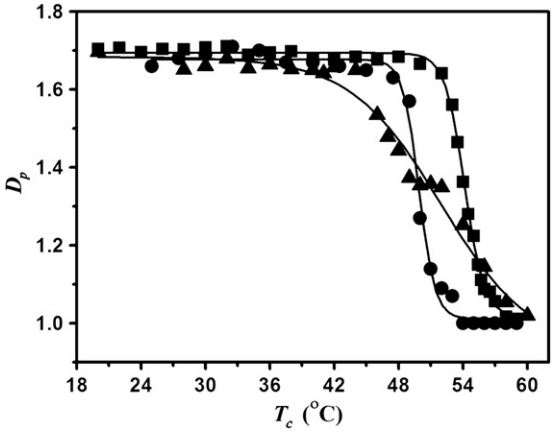

Fig. 4. Plots of D_p vs. T_c. ■ is 35k-PEO, ● is 5k-PEO and ▲ is the blend.

However, when we measured the thickness of different crystals, we found that crystallization of the blend sample has some distinct characteristics. Moreover, co-crystallization and molecular segregation have been observed. In Fig. 5 we selectively represent a three-dimensional image of the crystal pattern formed by the blend sample at $T_c = 49.0$ °C. Different thicknesses between the center and edge parts of the pattern are visible here. Interestingly, the patterns with different thicknesses only appear within $47.0 \le T_c \le 54.0$ °C. In Fig. 6 we summarize the T_c-dependences of the thickness for the three samples. At low T_cs, three samples have a similar thickness. In order to display the thickness difference obviously, we chose the temperature range between 35 °C and 60 °C in Fig. 6. The 5k-PEO fraction shows a stepwise T_c-dependence of the thickness because of the quantized folds, while a continuous T_c-dependence of the thickness for 35k-PEO. For the blend the T_c-dependence of the thickness is unlike to the pure fractions. At $47.0 \le T_c \le 54.0$ °C, the 32.3 ± 0.45 nm thickness is

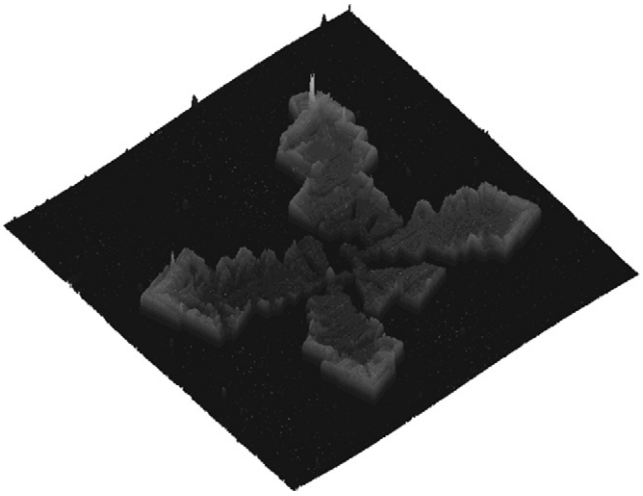

Fig. 5. 3D AFM image of a crystal pattern of the blend at $T_c = 49.0\ ^\circ C$.

measured from the crystal edges and it corresponds to the thickness of the fully extended-chain lamella of pure 5k-PEO. However, the thickness of the middle part or the backbone of the crystals is merely 20.8 ± 0.21 nm. This value is close to the non-integer fold chain lamella thickness of pure 35k-PEO. Therefore, we predict that the edge of the crystals may be constructed mainly by the extended-chain lamellae of the 5k-PEO fraction, whereas the middle part is mostly built up by the lamellae of the 35k-PEO fraction. This suggests that partial segregation may occur in this temperature region. When T_c is above 56.0 °C, the dual thickness disappears and the thickness is above 35.0 nm, moreover, it increases continuously with the crystallization temperature. In contrast with neat fractions, we suggest that the low molecular weight PEO molecules perhaps were completely rejected and full segregation occurred.

3.3. Co-crystallization

As we known, pattern formation in nonequilibrium crystallization significantly depends on the degree of undercooling ($\Delta T = T_m^0(MW) - T_c$, where $T_m^0(MW)$ is the equilibrium point, defined as the melting point of extended-chain crystals, $T_m(0)$). In our work, the undercooling for 5k-PEO is $\Delta T_1 = (62.2 - T_c)\ ^\circ C$, while, for 35k-PEO $\Delta T_2 = (67.8 - T_c)\ ^\circ C$ [58] (the subscripts 1 and 2 refer to the respective low- and high-molecular-weight components). At low T_cs (~45 °C and below), the degree of undercooling for both components is over 17 °C. In spite of the relative lower driving force and nucleation rate present for the 5k chains, the growth rate is higher than the 35k material, due to the smaller fold number in twice-, once-, or non-folded-chain crystals, while the fully chain-folded crystals associated with the higher molecular weight. Hence, the crystallization rates of the two PEO fractions are comparable and co-crystals formed at low crystallization temperatures. The unique thickness and the smooth surface of crystallization pattern indicated the blend was macroscopically homogenous after crystallization [59]. Moreover, upon the slow AFM heating experiments, we have obtained the single melting temperature of the co-crystals in the films, which provided the strong evidence to prove the blend co-crystallized on cooling. $D_p = 1.68 \pm 0.02$ clearly proves that diffusion of polymer chains from the surrounding melt to the growth front is the determining factor for co-crystal growth.

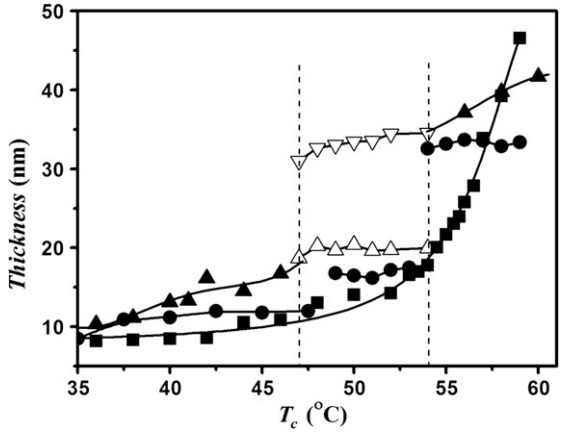

Fig. 6. Plots of thickness vs. T_c. ■ is 35k-PEO, ● is 5k-PEO and ▲ is the average thickness of the blend. ▽ is the edge thickness of the blend and Δ is the center thickness of the blend.

3.4. In-situ observation of partial segregation

At higher crystallization temperatures ($47.0 \le T_c \le 54.0\ ^\circ C$), the crystal patterns with different thicknesses were first observed. In the same T_c, the diverse thicknesses and shapes between the center and edges of a pattern indicates molecular segregation happened. In our experiment, 47.0 °C is the beginning segregation temperature and it is consistence with the segregation temperature of 4.5k-PEO in bulk state obtained by Chen et al [8]. In order to have a depth understanding of partial segregation, we examined the crystal growth by an in-situ AFM observation at $T_c = 54.0\ ^\circ C$. Choose the high crystallization temperature is due to the relative slow crystallization rate, so it is convenient for the track of crystal growth on AFM.

Fig. 7 shows the time evolution of the growing crystal. Fig. 7a corresponds to the initial stage of the nucleation. With elapse of time, the crystal grows in the radial direction with the finger-like shape as shown in Figs. 7b–d. Presented in Fig. 7c, the backbone of the crystal is relative darker, indicating the thickness of the backbone is thinner than that of the crystal edges. Figs. 7d and 7e demonstrate the formation of the square edges. At the final stage the crystal has the thin backbone and the thickening edges with a square shape (Fig. 7f). Such in-situ observation makes clear that the thin backbone forms first and grows fast while the square shape edges emerge later and will be thickened given enough crystallization time.

By analyzing the fractal dimension of the crystal, we can divide the crystallization process into two regions (I to II), as shown in Fig. 8. At $t < 7380$ s (region I), S and D_p increase rapidly with t and D_p has a maximum at $t = 7380$ s. At $t > 7380$ s (region II), S increases slowly with t, while D_p decreases slightly with t and then the values are close to a constant. From Fig. 7d, it can be seen that at $t = 7380$ s, part edges become square, thus we believe that the decrease of D_p is result from the formation of square crystals at edges.

To clarify the essence in region I, in Fig. 9 we plot the distance $R(t)$ at time t from the center of the nucleation site to the tip of the backbone with a maximum growth rate. We chose two different tips along the arrow direction shown in Fig. 7d. The linear relationship between $R(t)$ and $t^{0.5}$ is particularly interesting, which refers to a diffusion limited crystal growth at $t < 7380$ s. It should be noted that according to fractal length-area relation [55], $R^{D_p} \propto S$, due to the fractal characteristics of the crystal pattern we obtained, $D_p \neq 2$, it can clearly explain the nonlinear relationship between S and time.

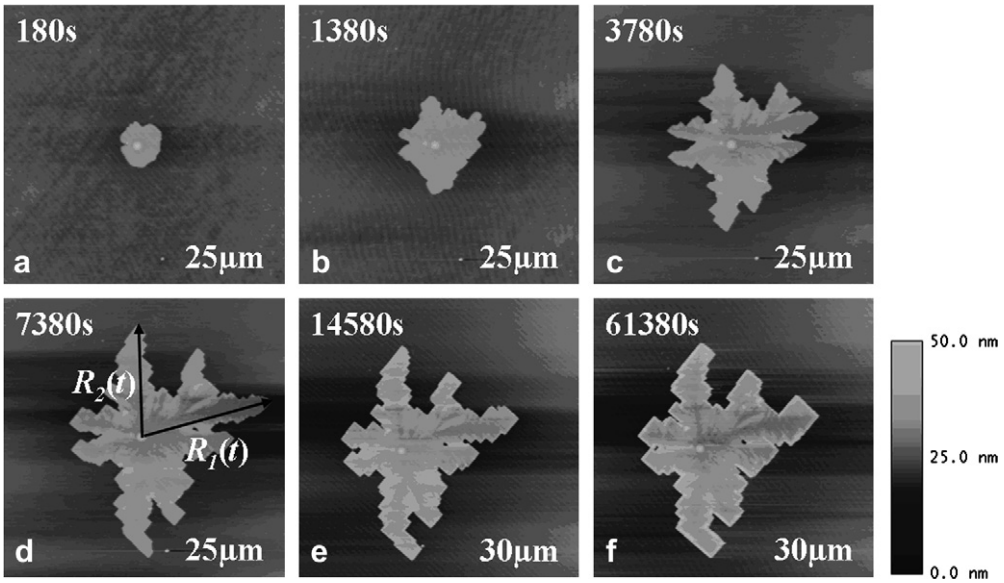

Fig. 7. Time evolution of the growing crystal observed by in-situ AFM observation.

Fig. 10 represents the time evolution of the growth length and the growth rate of the longest branch of the crystal studied in this experiment. In region I the time evolution of the growth rate of this single branch may be further divided into two sub-regions, I(a) and I(b). The growth rate is almost a constant, 0.00128 μm/s in sub-region I(a), justifying the growth governed by diffusion. At $t > 6000$ s, the growth rate decreases suddenly and the average rate is only 5.56×10^{-4} μm/s, indicating that the diffusion growth in sub-region I(a) is hindered by the other process. With an increase of time, the rate gradually decreases to zero. It is obvious that growth rates of these patterns in this temperature region are not linear.

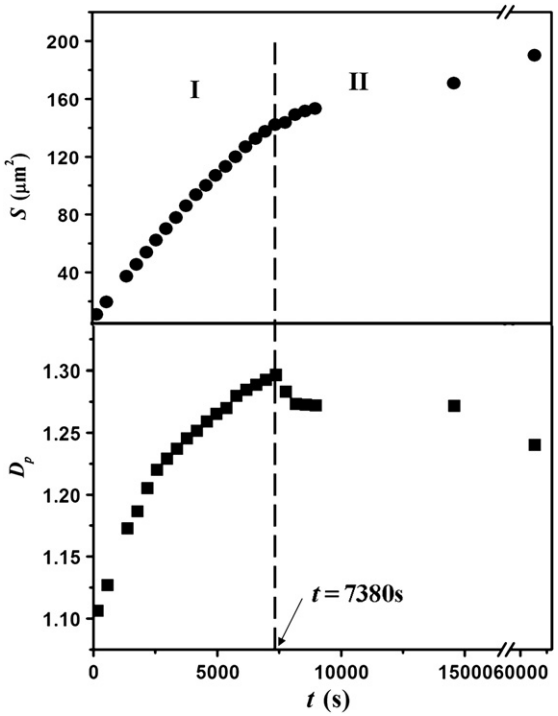

Fig. 8. Time dependence of D_p and the area S of the crystal.

3.5. Mechanism of pattern formation in partial segregation

Compared with short chain molecules, long chain molecules have lower segmental mobility, and a greater degree of undercooling brings higher nucleation ability, two opposing effects on the crystallization rate. The interplay between these two will determine the observed crystal morphology.

According to the kinetic crystallization theory [60], it is reasonable for PEO blends to form the crystals with dual thicknesses at intermediate crystallization temperatures. Kinetic crystallization theory yields the following relationship for the thickness of crystals (l^*) formed initially at a given T_c: $l^* = \frac{2\sigma_e}{\Delta F} + \delta$ (σ_e: the fold surface energy; ΔF the gain in free energy density which is proportional to the quench depth ΔT; δ is the thickness that gives the crystals the necessary stability to form by creating a situation where the free energy of crystal formation is negative). While, for PEO and PE, which can crystallize fairly rapidly at a low undercooling to yield thick lamellae, the δ value would make a negligible contribution to l^*[61]. Comparing 5k-PEO with 35k-PEO, $\sigma_e(35k) < \sigma_e(5k)$, $\Delta F(35k) > \Delta F(5k)$, hence, $l^*(5k) > l^*(35k)$. A

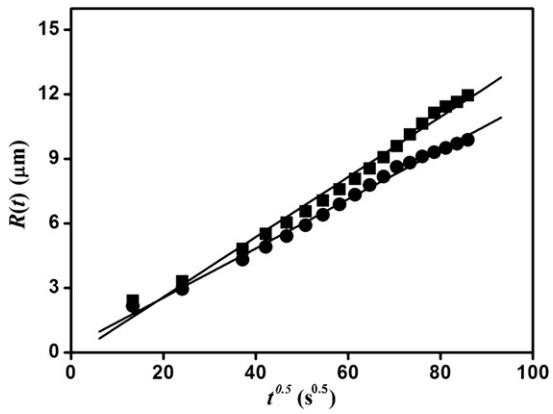

Fig. 9. Plots of $R(t)$ (indexed in Fig. 7d) vs. crystallization time $t^{0.5}$ in regime I. ■ represents the branch growth directed by $R_1(t)$ as shown in the Fig. 7d, and the solid line is the line fitting of $R_1(t)$, $R = 0.9943$; ● represents the branch growth directed by $R_2(t)$ as shown in the Fig. 7d, and the solid line is the line fitting of $R_2(t)$, $R = 0.9972$.

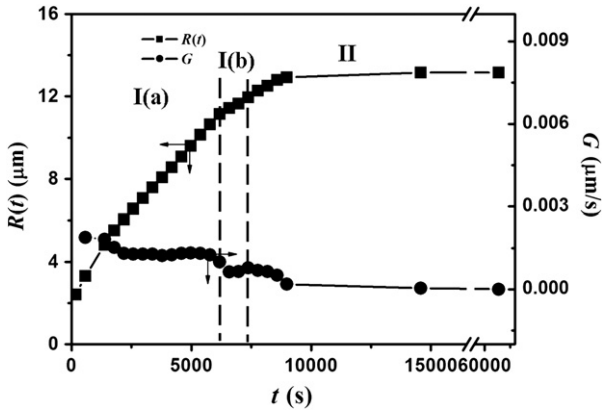

Fig. 10. Plots of $R(t)$ (blue arrow indexed in Fig. 7d) and the corresponding growth rate G vs. crystallization time t. ■ is $R(t)$ and ● represents G.

simplifying assumption often made is that the final lamellar thickness (L) is β times larger than the initial thickness (l^*). As to PEO blend, with increasing crystallization temperature, $\Delta l^*\uparrow$, $\Delta L\uparrow$, hence, finally PEO blend formed the crystal with dual lamellar thicknesses.

Based on previous literature and the results we have obtained, we suggest a possible pattern formation mechanism which is schematically summarized in Fig. 11.

Fig. 11a and b describe the 35k-PEO growth in sub-region I(a). Fig. 11a depicts the first step of the pattern formation by nucleation and dendrite growth of 35k-PEO. Following the crystal-nucleation theory [12], the free energy barrier for intramolecular secondary nucleation is calculated as $\Delta F_{c2D} = \sigma_{2D}^2/4\Delta f_{2D}$, where σ_{2D} is a constant corresponding to the surface free energy density and absorbing all the prefactors, and Δf_{2D} is roughly proportional to the undercooling. This equation predicts that the height of free energy barrier has a reciprocal dependence on the undercooling. With the same T_c, the 35k-PEO chains have larger ΔT due to the higher $T_m^0(MW)$. As T_c increases, the relative undercooling discrepancy $\Delta T_2/\Delta T_1$ of the two components becomes larger, from 1.17 (at $T_c = 30\,^\circ$C, $\Delta T_2 = 37.8\,^\circ$C and $\Delta T_1 = 32.2\,^\circ$C) to 1.42 (at $T_c = 49.0\,^\circ$C, $\Delta T_2 = 18.8\,^\circ$C and $\Delta T_1 = 13.2\,^\circ$C), thus, nucleation exerts more considerable influence on the crystallization. The 35k-PEO chains have smaller free enthalpy barrier for nucleation, suggesting that long chains facilitate nucleation. On the other hand, the free energy barrier for melting of single chains on the crystal growth front is $\Delta F_{m2D} = N\Delta f_{2D} - \sigma_{2D}N^{1/2} + \sigma_{2D}^2/4\Delta f_{2D}$ [12], which shows significant chain length dependence. The longer the chains are, the higher the barrier for melting is. Therefore, long chains can survive in the intramolecular secondary nucleation and contribute to the advancing of the crystal growth front while low molecular mass PEO molecules are initially rejected. Then the 35k chains began fractal growth governed by DLA model and formed the backbone of the patterns, as presents in Fig. 11b. The thickness of backbone is 20.8 nm averagely that is close to the non-integer fold chain lamella thickness of the 35k-PEO fraction. And the relationship of $R(t) \propto t^{0.5}$ confirms that the diffusion limited process mainly governed the backbone growth. However, this process cannot go very far, since the rejected low molecular mass PEO molecules are accumulating in the growth front of the crystals and soon, a probability of the appearance of the high molecular mass PEO at the growth front decreases. The faster growing component (the high molecular weight polymer) provides nucleation sites for the addition of low molecular weight component as Fig. 11c shown. The diffusion growth of 35k-PEO is influenced by adding the 5k-PEO, thus the branch tip growth rate decreases suddenly in sub-region I(b). Fig. 11d represents the formation of pattern edges with a regular shape mostly built by 5k-PEO. Theoretically, diffusion coefficient D is proportional to $M_n^{-\alpha}$, and for PEO, when $M_n < 7000$ g/mol, $\alpha = 1$, while, $M_n > 7000$ g/mol, $\alpha = 2.3$ [62]. So, $D_{5k}/D_{35k} \approx 5000^{-1}/35000^{-2.3} = 5.6 \times 10^6$, the diffusion rate of the 35k chains is definitely much less than short chains, thus, it is much easier for the 5k chains to diffuse to nucleation sites and grow. Because of the high crystallization temperature, the movement ability of 5k-PEO molecules enhances and molecules have enough energy to overcome free energy barrier to form more stable and regular crystals in the pattern periphery. However, the growth of this stable crystal needs more time due to the adjustment of PEO chains; thus, the growth rate in region II is very low. Based on the previous work [25], we consider that the edge growth of 5k-PEO is mainly controlled by the surface nucleation. However, since the concentration of different molecules in the growth front is changeable, we have to admit that it is unlikely that this crystal layer of the pattern periphery consists of molecules of low-molar-mass only. And it should be noted that the growth of 5k-PEO molecules are companied with some 35k-PEO molecules.

Although a general mechanism of pattern formation has been suggested, it is worthy to discuss the final segregation pattern in details in order to have a more comprehensive understanding. As to the trunk, when $T_c = 48.0$ and $49.0\,^\circ$C the width of the fractal trunk is less than the width of co-crystals that formed at low temperatures, which is abnormal to the trend that the width of the pattern is increasing with the rising temperature. It was shown that an increase in molecular mass promotes the nucleation rate much more significantly compared with its effect on the growth rate and this in turn leads to a higher nucleation density [63]. Hence, in order to explain the thin trunk, we assume in the melt, short chains with good diffusion ability blocked long chain movement. And large steric effect also obstructed the trunk growth when the growth front was once surrounded by 5k-PEO.

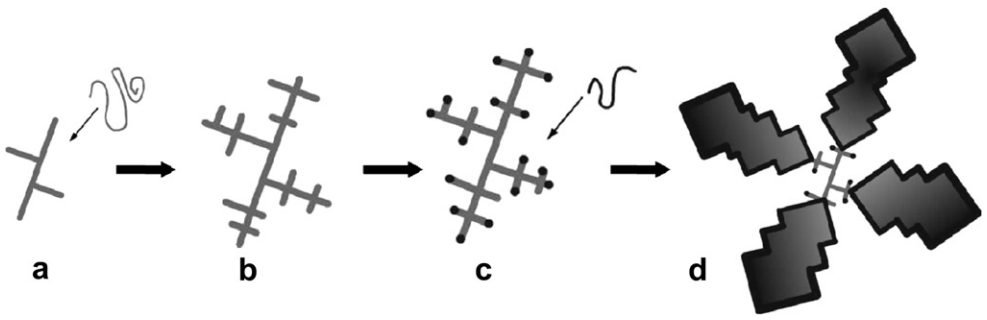

Fig. 11. A suggested scheme showing the effect of molecular segregation on pattern formation. (a) Nucleation of 35k-PEO; (b) Growth of 35k-PEO crystals controlled by DLA; (c) Nucleation of 5k-PEO on the tips of 35k-PEO crystals; (d) Periphery growth of 5k-PEO crystals.

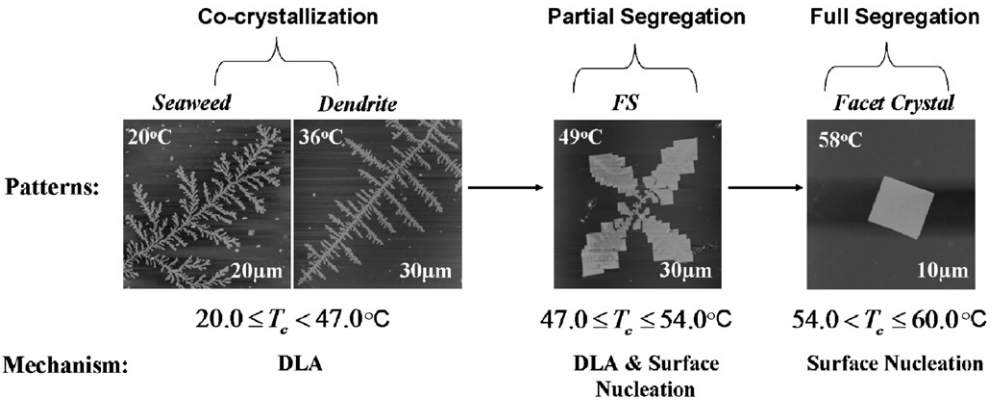

Fig. 12. Demonstration of a unified scheme to show the different crystal patterns and mechanisms of binary mixtures of PEO fractions, according to the crystallization temperature.

We have known that pure 5k-PEO crystals become faceted with a regular square shape about 54.0 °C [37], then, how to elucidate that 5k-PEO has already formed the faceted crystals at 47.0 °C in the blend system? In our opinion, the most important factor is the nucleation sites offered by long chain molecules. In other words, the long chains greatly improve the crystallization ability of short chains.

In our system, beside of the diverse motion and nucleation abilities of the two components, several other factors such as blend effect and ultra-thin film constraint should also be considered in order to account for the faceted crystal formation at relative low temperatures compared to the neat component. First, based on the modification of Flory-Huggins expression [8,64,65], we calculated the melting temperatures of the two components, $T_{m1} = 335.1$ K (61.9 °C) and $T_{m2} = 340.3$ K (67.1 °C), respectively. It should be noted that blending two fractions would slightly decrease the melt point of the components. Besides, substrate effect on the melting temperature also cannot be neglected. Previous study indicates that the T_m decreases with the film thickness decrease and films melt 5–38 °C below the bulk values depending on film thickness [66]. And this is unique in the long chain molecule system since the tendency for randomly adsorbing the chain and breaking the order is less possible for the small molecules due to the short chain length. In our case, as to 5k-PEO sample, the $T_m(0)$ of 5k-PEO were measured to be 62.0 °C and hence the effect of the substrate on T_m is slight. As to 35k-PEO sample, we cannot obtain the extended-chain crystals and the highest crystallization temperature at which we can obtain 35k-PEO crystals is 59.0 °C, meaning that the strong substrate attraction force perhaps decrease the T_m of 35k-PEO. On the other words, the movement ability of the 35k-PEO is decreased greatly compared to 5k-PEO. It also contributes to the formation of the facet crystal for 5k-PEO at relative low T_cs.

Finally, we would like to mention two computer simulations on the influence of particle size on pattern formation resulted by random DLA model [22,23]. In these works a few large particles are mixed in the small particles, the final cluster pattern appears asymmetrical and large particles become new growth centers around which other small particles grow and form new branches. Our observations of the special patterns in the partial segregation range are qualitatively similar with the computer simulations and we considered that the high molar mass component plays a significant role as the center of crystallization pattern.

3.6. Full segregation

When T_c is above 56 °C, crystals with regular shape and almost uniform thickness were observed. Measured the crystal thickness, as shown in Fig. 6, we noticed that the thickness of these crystals increases continuously with the crystallization temperature. The regular shape crystals, similar with single crystals, grow under the surface nucleation control. Thus, we suggest that in high crystallization temperature region, the low molecular weight PEO molecules are completely rejected and sole crystallization of high molecular weight PEO molecules causes a full segregation. Short chain fractions are fully excluded by their failures on the intramolecular secondary nucleation for crystal growth. However, the crystal thickness is not the same as the thickness of the neat 35k-PEO crystals. Blend effect and the molecular weight distribution of 5k-PEO perhaps could be employed to explain this experimental result.

4. Conclusion

In summary, we have presented our AFM results imaging the crystal patterns of 5k-PEO and 35k-PEO blends (50/50 wt) at different T_cs. We found the common and specific pattern features among the neat components and the blend, and discussed the different mechanisms of pattern formation for the blend sample crystallization in the co-crystallization, partial and full segregation regions, as shown in Fig. 12.

Thin film crystallization of these three polymers is mainly controlled by a competition of molecular diffusion and surface nucleation. At low temperatures, diffusion governs the ramified pattern formation; while surface nucleation is the main mechanism in high temperature range. As to the blend, the movement of different molecules becomes more complex. The study of D_p and thickness indicates that both components co-crystallize at high undercoolings. The seaweed and dendrite patterns were observed at low T_cs. They have the similar fractal dimension $D_p = 1.68 \pm 0.02$ on average, meaning that the diffusion controlled aggregation is the underlying mechanism. When T_c is enough high, the full segregation occurred and the low molecular weight PEO molecules were rejected. However, at $47.0 \le T_c \le 54.0$ °C, partial molecular segregation has been reported. Utilizing in-situ AFM equipment in the tapping mode to follow the isothermal crystal growth at 54.0 °C, we suggested a growing mechanism for dual thickness crystals. We considered that at first, high molecular weight chains are easier to nucleate compared to the low molecular weight due to the larger driving force available to them and crystals grow under control mainly by DLA model to form the dendritic backbones of crystal patterns. The grown trunks provide nucleation sites for the addition of short chains. Finally, short chains mainly build up the edge parts of patterns with square shape and extended-chain lamellae of 5k-PEO, governed by the surface kinetic process. These results

provide a number of immediate directions for detailed studies of molecular segregation in polymeric systems and the role of molecular weight in polymer crystallization.

Acknowledgement

We greatly appreciate National Science Foundation of China for grants (NSFC20474033 and 20874053) to support this work.

References

[1] Wunderlich B. Macromolecular physics. New York: Academic; 1976.
[2] Gedde UW. Polymer physics. London: Chapman and Hall; 1995.
[3] Schultz JM. Polymer crystallization. Oxford: Oxford University Press; 2001.
[4] Bank MI, Krimm S. J Polym Sci B 1970;8:143–8.
[5] Wunderlich B, Mebta A. J Polym Sci Polym Phys Ed 1974;12:255–63.
[6] Mebta A, Wunderlich B. Colloid Polym Sci 1975;253:193–205.
[7] Wunderlich B. Faraday Discuss Chem Soc 1979;68:239–43.
[8] Cheng SZD, Wunderlich B. J Polym Sci Polym Phys Ed 1986;24:577–94.
[9] Cheng SZD, Wunderlich B. J Polym Sci Polym Phys Ed 1986;24:595–617.
[10] Cheng SZD, Bu HS, Wunderlich B. J Polym Sci Polym Phys Ed 1988;26:1947–64.
[11] Balijepalli S, Schultz JM. Macromolecules 1996;29:6601–11.
[12] Hu WB, Frenkel D, Mathot VBF. Macromolecules 2003;36:8178–83.
[13] Hu WB. Macromolecules 2005;38:8712–8.
[14] Langer JS. Rev Mod Phys 1980;52:1–28.
[15] Meakin P. Fractals, scaling and growth far from equilibrium. Cambridge: Cambridge University Press; 1997.
[16] Kassner K. Pattern formation in diffusion-limited crystal growth. Singapore: World Scientific; 1996.
[17] Saito Y. Statistical physics of crystal growth. Singapore: World Scientific; 1996.
[18] Libbrecht KG. Rep Prog Phys 2005;68:855–95.
[19] Mullins WW, Sekerka RF. J Appl Phys 1964;35:444–51.
[20] Witten TA, Sander LM. Phys Rev Lett 1981;47:1400–3.
[21] Witten TA, Sander LM. Phys Rev B 1983;27:5686–93.
[22] Ossadnik P, Lam CH, Sander LM. Phys Rev E 1994;49:R1788–91.
[23] Tan ZJ, Zou XW, Zhang WB, Jin ZZ. Phys Rev E 1999;60:6202–5.
[24] Brener E, Muller-krumbhaar H, Temkin D. Europhys Lett 1992;17:535–40.
[25] Saito Y, Ueta T. Phys Rev A 1989;40:3408–19.
[26] Bogoyavlenskiy VA, Chernova NA. Phys Rev E 2000;61:1629–33.
[27] Provatas N, Wang QY, Haataja M, Grant M. Phys Rev Lett 2003;91:155502–4.
[28] Honjo H, Ohta S, Matsushita M. Phys Rev A 1987;36:4555–8.
[29] Gránásy L, Pusztai T, Börzsönyi T, Warren JA, Douglas JF. Nat Mater 2004;3:645–50.
[30] Lovinger AJ, Cais RE. Macromolecules 1984;17:1939–45.
[31] Reiter G, Sommer JU. Phys Rev Lett 1998;80:3771–4.
[32] Reiter G, Sommer JU. J Chem Phys 2000;112:4376–83.
[33] Taguchi K, Miyaji H, Izumi K, Hoshino A, Miyamoto Y, Kokawa R. Polymer 2001;42:7443–7.
[34] Zhang F, Liu J, Huang H, Du B, He T. Eur Phys J E 2002;8:289–97.
[35] Ferreiro V, Douglas JF, Warren JA, Karim A. Phys Rev E 2002;65:042802–4.
[36] Ferreiro V, Douglas JF, Warren JA, Karim A. Phys Rev E 2002;65: 051606–16.
[37] Zhai XM, Wang W, Zhang GL, He BL. Macromolecules 2006;39:324–9.
[38] Zhai XM, Wang W, Ma ZP, Wen XJ, Yuan F, Tang XF, et al. Macromolecules 2005;38:1717–22.
[39] Li BB, Esker AR. Langmuir 2007;23:2546–54.
[40] Wang MT, Braun HG, Meyer E. Macromolecules 2004;37:437–45.
[41] Okerberg BC, Marand H. J Mater Sci 2007;42:4521–9.
[42] Okerberg BC, Marand H, Douglas JF. Polymer 2008;49:579–87.
[43] Ma ZP, Zhang GL, Zhai XM, Jin LX, Tang XF, Yang M, et al. Polymer 2008;49:1629–34.
[44] Meyer E, Braun H- G. J Phys Condens Matter 2005;17:S623–35.
[45] Zhang GL, Jin LX, Ma ZP, Zhai XM, Yang M, Zheng P, et al. J Chem Phys 2008;129:224708.
[46] Neelakandan C, Kyu T. Polymer 2009;50:2885.
[47] Fenouillot F, Cassagnau P, Majesté JC. Polymer 2009;50:1333.
[48] Ogawa H, Kanaya T, Nishida K, Matsuba G. Polymer 2008;49:254.
[49] Qiao C, Zhao JC, Jiang SC, Ji XL, An LJ, Jiang BZ. J Polym Sci Polym Phys Ed 2005;43:1303–9.
[50] Arlie P, Spegt PA, Skoulios A. Makomol Chem 1966;99:160–74.
[51] Arlie P, Spegt PA, Skoulios A. Makomol Chem 1967;104:212–29.
[52] Spegt PA. Makromol Chem 1970;139:139–52.
[53] Zhu DS, Liu YX, Chen EQ, Li M, Chen C, Sun YH, et al. Macromolecules 2007;40:1570–8.
[54] Schönherr H, Bailey LE, Frank CW. Langmuir 2002;18:490–8.
[55] Mandelbrot BB. The fractal geometry of nature. San Francisco: W.H. Freeman and Company; 1982.
[56] Kaye BH. A random walk through fractal dimension. New York: VCH Publishers; 1989.
[57] Banavar JR, Kohmoto M, Roberts J. Phy Rev A 1986;33:2065–7.
[58] Equilibrium melting points of 5k-PEO and 35k-PEO were calculated using the Flory-Vrij relation. Using the in-situ AFM with a hot stage, we have determined the melting temperature of the extended-chain crystals for 5K-PEO sample in ultra-thin films, $T_m(0) = T_m^0(5k) = 62.0\,^{\circ}C$, consistent with the calculated value. As to 35k-PEO, extended-chain crystals cannot be obtained experimentally. The equilibrium melting temperature for the crystalline form of 35k-PEO is obtained through extrapolative procedures.
[59] Kirkland BS, Paul DR. Polymer 2008;49:507–24.
[60] Hoffman JD, Davis GT, Llauritzen JI. Treatise on solid state chemistry. New York: Plenum Press; 1975.
[61] Hoffman JD, Miller RL. Polymer 1997;38:3151–212.
[62] Rubinstein ER, Colby RH. Polymer physics. New York: Oxford University Press Inc; 2003.
[63] Chen HL, Li LJ, Ou-Yang WC, Hwang JC, Wong WY. Macromolecules 1997;30:1718–22.
[64] Flory PJ, Vrij A. J Am Chem Soc 1963;85:3548–53.
[65] Cheng SZD, Chen J, Janimak JJ. Polymer 1990;31:1018–24.
[66] Wang Y, Rafailovich M, Sokolov J, Gersappe D, Araki T, Zou Y, et al. Phys Rev Lett 2006;96:028303.